AIAA JOURNAL
Vol. 46, No. 3, March 2008

Cylindrical Shell Submerged in Bounded Acoustic Media: A Modal Approach

R. Benjamin Davis* and Lawrence N. Virgin†
Duke University, Durham, North Carolina 27708
and
Andrew M. Brown‡
NASA Marshall Space Flight Center, Huntsville, Alabama 35812

DOI: 10.2514/1.31706

The dynamics of a simply supported cylindrical shell submerged in liquid hydrogen and liquid oxygen are considered. The shell itself is bounded by a rigid outer cylinder with closed rigid ends. This configuration gives rise to two fluid-filled cavities—an inner cylindrical cavity and an outer annular cavity. Such geometries are common in rocket engine design. The natural frequencies and modes of the fluid-structure system are computed by combining the rigid wall acoustic cavity modes and the in vacuo structural modes into a system of coupled ordinary differential equations. Eigenvalue veering is observed near the intersections of the curves representing natural frequencies of the rigid wall acoustic and the in vacuo structural modes. In the case of a shell submerged in liquid hydrogen, system frequencies near these intersections are as much as 30% lower than the corresponding in vacuo structural frequencies. Because of its high density, the frequency reductions in the presence of liquid oxygen are even more dramatic. The forced responses of a shell submerged in liquid hydrogen and liquid oxygen, while subject to a harmonic point excitation, are also presented. The responses in the presence of fluid are found to be quite distinct from those of the structure in vacuo.

Nomenclature

A	=	surface area of shell calculated at middle surface
$[A]$	=	system matrix, see Eq. (33)
A_F	=	surface area of shell calculated at fluid interface
a	=	acoustic modal coordinate (units of velocity potential)
a_0	=	radius of shell measured from origin to middle surface
$[B]$	=	see Eq. (33)
$[C]$	=	damping matrix
c	=	complex modal force transformation factor, see Eq. (38)
c_0	=	speed of sound in fluid
D, D	=	intermediate modal force, modal force, see Eqs. (39) and (40)
$d_{0,1,2}$	=	coefficients of shell characteristic equation, see Eqs. (A.6), (A.7), and (A.8)
E	=	Young's modulus
F	=	acoustic normal mode (with subscript), forcing amplitude (without subscript)
$[G]$	=	gyroscopic matrix
$\mathbf{g}$	=	generalized coordinates that may contain both fluid and structural degrees of freedom
h	=	thickness of shell structure
K	=	index number of highest-order acoustic mode retained in frequency calculation
$[K]$	=	stiffness matrix
$k_{n_a p_a}$	=	roots of the characteristic equation for a rigid annular cavity, see Eq. (9)
L	=	acoustic-structure coupling coefficient, see Eq. (21)
ℓ	=	shell length
M	=	generalized modal mass
$[M]$	=	mass matrix
M_a, N_a, P_a	=	index numbers of the highest axial, circumferential, radial modes retained
M_s, N_s	=	index numbers of the highest axial, circumferential modes retained
m_a, n_a, p_a	=	acoustic axial, circumferential, radial wave numbers
m_s, n_s	=	structural axial, circumferential wave numbers
$\mathbf{Q}$	=	forcing vector
q	=	structural modal coordinate (units of displacement)
R_i, R_o	=	inner, outer radius of fluid cavity
r	=	radial direction in cylindrical-polar coordinate system
$\mathbf{r}$, $\mathbf{s}$	=	real, imaginary parts of right eigenvectors, see Eq. (37)
t	=	time
$\mathbf{u}$, $\mathbf{v}$	=	real, imaginary parts of left eigenvectors, see Eq. (37)
u, v, w	=	shell axial, circumferential, and radial displacements
V	=	volume of fluid cavity
X	=	radial displacement amplitude of forced shell
$\mathbf{X}$, $\mathbf{Y}$	=	right, left eigenvectors
$\mathbf{x}$	=	state vector, see Eq. (33)
Z	=	number of degrees of freedom in system equations of motion, see Eq. (31)
z	=	axial direction in cylindrical-polar coordinate system

Presented as Paper 2110 at the 48th AIAA/ASME/ASCE/AHS/ASC Structures, Structural Dynamics, and Materials Conference, Honolulu, Hawaii, 23–26 April 2007; received 19 May 2007; revision received 5 September 2007; accepted for publication 18 September 2007.

*Graduate Research Assistant, Department of Mechanical Engineering and Materials Science. Student Member AIAA.
†Professor and Chair, Department of Civil and Environmental Engineering. Senior Member AIAA.
‡Aerospace Engineer, Structural and Dynamics Analysis Branch. Senior Member AIAA.

α, β = real, imaginary parts of eigenvalues, see Eq. (37)
$\alpha'_{n_a p_a}$ = roots of characteristic equation for rigid cylindrical duct, that is, $J'_{n_a}(\alpha'_{n_a p_a}) = 0$
Γ = radial variation of rigid wall acoustic mode in an annulus, see Eq. (12)
γ = structural parameter, see Eq. (A.5)
δ_{n_a} = 1 if $n_a = 0$, =0 otherwise
ε_{m_a} = 1 if $m_a = 0$, =2 otherwise
$\varepsilon_{n_{s,a}}$ = 1 if $n_{s,a} = 0$, =2 otherwise
ζ = damping ratio
θ = circumferential direction in cylindrical-polar coordinate system
λ = eigenvalue
μ = structural parameter, see Eq. (A.9)
ν = Poisson's ratio
ξ = frequency shift parameter
ϖ = natural frequency of acoustic cavity
ρ_s, ρ_0 = mass density of structure, fluid
σ = structural parameter, see Eq. (A.4)
Φ = fluid velocity potential
Ψ = structural normal mode
Ω = structural natural frequency
$\bar{\Omega}$ = structural frequency parameter $\equiv a_0\sqrt{[\rho_s(1-\nu^2)/E]}\Omega$
ω = angular frequency

Conventions

n = normal direction
$[I]$ = identity matrix
i = imaginary unit $\equiv \sqrt{-1}$
$J_n(\circ)$ = nth Bessel function of the first kind of $(\circ)$
$Y_n(\circ)$ = nth Bessel function of the second kind (a.k.a. Neumann function) of $(\circ)$
δ_{ij} = Kronecker delta, =1 if $i = j$, =0 otherwise
$\nabla^2(\circ)$ = Laplacian operator of $(\circ)$
$[\circ]^T$ = matrix or vector transpose of $[\circ]$
$[\circ]^{*T}$ = complex conjugate transpose of $[\circ]$
$(\circ)'$ = derivative of $(\circ)$ with respect to either r (Bessel functions) or z (shell equations of motion)
$(\circ)^{\cdot}$ = partial derivative of $(\circ)$ with respect to θ
$(\dot{\circ})$ = first derivative of $(\circ)$ with respect to time
$(\ddot{\circ})$ = second derivative of $(\circ)$ with respect to time

Subscripts

I, R = imaginary, real
i, j = mode indices, see Eq. (36)
k = mode index, see Eq. (37)
max = maximum
m_a, n_a, p_a = acoustic axial, circumferential, radial wave numbers
m_s, n_s = structural axial, circumferential wave numbers
nat = natural
r, v = acoustic mode number indices

Superscripts

A = cavity A
B = cavity B
radial = radial component of structural normal mode

I. Introduction

LARGE-SCALE investigations related to the space shuttle have underscored the need to accurately model the interaction between acoustic energy and rocket engine components. In at least one recent instance, NASA has identified acoustic excitation in liquid propellant as a significant contributor to the high-cycle fatigue of an Orbiter component [1]. The effect of fluid on the dynamic response of a structure can be an important consideration when the structure is flexible and/or the fluid is relatively dense. Because liquid rocket engines possess a variety of flexible structures loaded with liquid fuels and oxidizers that are at least 50 times more dense than air, it is often necessary to analyze rocket engine components as coupled fluid-structure systems. In such systems neither pure structural modes nor pure acoustic cavity modes exist. Instead, the system natural modes receive contributions from both the acoustic cavity and the structure.

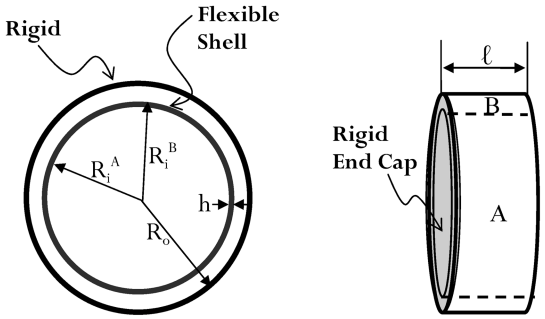

Fig. 1 Schematic of system.

The dynamics of a submerged simply supported cylindrical shell of finite length are considered. Because the fundamental features of acoustic-structure interaction are of primary interest here, simply supported boundary conditions were chosen for the relative analytical simplicity that they afford. In the case of a shell, simply supported boundary conditions indicate that the internal bending moment, the membrane normal force as well as the radial and circumferential (but not the axial) displacements are all equal to zero at both shell ends. The shell is submerged in a quiescent, inviscid, compressible fluid that is bounded by a rigid outer cylinder with closed rigid ends (see Fig. 1). This configuration gives rise to two acoustic cavities—an inner cylindrical cavity and an outer annular cavity. Such geometries are common in rocket engine design; indeed, the specific system considered here was motivated by the design of the space shuttle gimbal joint flowliner [1].

The remainder of this paper begins with a brief review of the relevant literature as well as a discussion of the new contributions of the present work. Sections III and IV present the mathematical formulation used to investigate the free and forced dynamics of the system. A presentation and discussion of the results can be found in Sec. V. This is followed by some concluding remarks which place the study within a broader context and discuss how researchers and rocket engine designers might make use of its results.

II. Background

A. Relevant Literature

The dynamics of structures containing fluid is a topic that has commanded long-standing interest among researchers. In the early 1960s, Warburton [2] was one of the first to recognize that a cylindrical shell containing air possesses resonant frequencies that are close to either the in vacuo structural natural frequencies or the rigid wall acoustic natural frequencies of the enclosed air. Dowell et al. [3] expanded upon this idea by developing a comprehensive theoretical model that combines the rigid wall acoustic cavity modes and the in vacuo structural modes into a system of coupled ordinary differential equations. This approach, which provides the theoretical framework for the present work, has been used to investigate sound-structure interaction in a variety of systems of practical interest including rectangular enclosures [4], airplane fuselages [5], and computer disk drives [6]. It is noted that the present work concerns the interaction of cylindrical shells with fluid that is bounded by the walls of a cavity. There is a vast literature that considers the interaction of flexible structures (including cylindrical shells) with

unbounded acoustic media (typically air or water). An interested reader may wish to consult the classic text of Junger and Feit [7].

Rocket engine components are not the only systems where cylindrical shells in bounded acoustic media are of interest. Au-Yang [8] studied a problem similar to the one considered here, but in the context of heat exchanger tubes and nuclear reactor vessel internals. His formulation, however, is limited in that it uses only hydrodynamic mass to account for fluid effects. This method is an efficient way to compute the fluid-loaded structural frequencies provided the frequencies of interest are not close to frequencies corresponding to an adjacent acoustic cavity. Forcing frequencies associated with the space shuttle main engine (SSME) gimbal joint flowliner are close to the intersection of acoustic cavity and structural resonances [1], thus a more general approach is applied here. Gardonio et al. [9] have taken such an approach in their consideration of fluid-filled cylindrical shells with blocking masses. Kruntcheva [10] and Molisani [11] have done likewise in their treatment of a problem that is nearly the inverse to the one studied here. They each considered the dynamics of an air-filled annular gap bounded by a flexible outer cylindrical shell and a rigid inner cylinder. Such a configuration is relevant to the analysis of automobile and aircraft tires.

B. Contributions

This study represents the first known investigation of the dynamics of a cylindrical shell that is coupled to both cylindrical and annular fluid-filled cavities. The present study is also unique in that it considers liquid hydrogen (LH_2), a common rocket fuel, and liquid oxygen (LOX), a common oxidizer, in a coupled fluid-structure system. Given their ubiquity in the physical world, it is understandable that virtually all existing fluid-structure interaction studies consider either air or water as the fluid of interest. In the case of air, it is rare for the inclusion of fluid coupling to dramatically affect the structural dynamic response. However, because of water's substantial density, a water-loaded structure will generally have natural frequencies that are much lower than the corresponding structure in vacuo. For many water-loaded structures of practical interest, these hydrodynamic effects tend to dominate any effects resulting from acoustic coupling (the same can be said for structures loaded with LOX). However, with a density that is about 58 times that of air, but about 14 times less than that of water, LH_2 falls into a middle range where both hydrodynamic and acoustic effects are important considerations. The manner in which these two effects contribute to the overall dynamic response of the system is discussed in Sec. V.

Because of gyroscopic coupling between the fluid and the structure, calculating the forced response of the system of interest requires a nonsymmetric eigenanalysis. Bokil and Shirahatti [4] presented a procedure for determining the forced response of coupled acoustic-structure systems, but their formulation is based on undamped equations of motion and is thus of limited practical use when attempting to assess the relative amplitudes of the system response across a range of frequencies. In this study, a procedure has been adapted from Meirovitch [12] and from Patil [13] to transform the damped acoustic-structure equations of motion into an uncoupled second-order form. Such a form is desirable because it allows for the use of familiar modal analysis techniques to generate forced response curves.

III. Theoretical Model

In this section, the rigid wall acoustic and in vacuo structural natural frequencies and mode shapes are treated individually and then assembled into a set of coupled equations of motion.

A. Acoustic Model

The fluid residing in the cylindrical and annular cavities is assumed to obey the linear, homogeneous wave equation,

$$\nabla^2\Phi - \frac{1}{c_0^2}\frac{\partial^2\Phi}{\partial t^2} = 0 \tag{1}$$

which is written in terms of the velocity potential Φ. With rigid wall boundary conditions, solutions to Eq. (1) are given by the normal modes, $F_r e^{i\varpi_r t}$ $(r = 0, 1, 2, 3, \ldots)$, which satisfy

$$\nabla^2 F_r + \left(\frac{\varpi_r}{c_0}\right)^2 F_r = 0 \tag{2}$$

$$\frac{\partial F_r}{\partial \mathbf{n}} = 0, \qquad \text{on wall} \tag{3}$$

The normal modes also satisfy the orthogonality relation,

$$\frac{1}{V}\int_V F_r F_v \,\mathrm{d}V = 0 \qquad r \neq v$$
$$= M_r, \qquad r = v \tag{4}$$

The rigid wall natural frequencies and modes corresponding to cylindrical and annular acoustic cavities are well known and can be found in (or derived with the aid of) most general acoustics texts (see, e.g., Blackstock [14]). For a rigid cylindrical duct (cavity A) it can be shown that the normal modes, the acoustic natural frequencies, and generalized modal mass are given by

$$F^A_{m_a n_a p_a} = J_{n_a}\left(\alpha'_{n_a p_a}\frac{r}{R_i^A}\right)\cos(n_a\theta)\cos\left(\frac{m_a\pi}{\ell}z\right) \tag{5}$$

$$\varpi^A_{m_a n_a p_a} = c_0\sqrt{\left(\frac{\alpha'_{n_a p_a}}{R_i^A}\right)^2 + \left(\frac{m_a\pi}{\ell}\right)^2} \tag{6}$$

$$M^A_{m_a n_a p_a} = \frac{1}{\varepsilon_{n_a}\varepsilon_{m_a}}\left[1 - \left(\frac{n_a}{\alpha'_{n_a p_a} + \delta_{n_a}}\right)^2\right]J^2_{n_a}(\alpha'_{n_a p_a}) \tag{7}$$

respectively. Here the index r has been expanded to explicitly show its axial (m_a), circumferential (n_a), and radial (p_a) components. In the case of the annular cavity (cavity B), the rigid wall natural frequencies are

$$\varpi^B_{m_a n_a p_a} = c_0\sqrt{\left(\frac{k_{n_a p_a}}{R_i^B}\right)^2 + \left(\frac{m_a\pi}{\ell}\right)^2} \tag{8}$$

where $k_{n_a p_a}$ denote the roots of the characteristic equation for a rigid annular cavity, that is,

$$k^2_{n_a p_a}\left[Y'_{n_a}\left(k_{n_a p_a}\frac{R_o}{R_i^B}\right)J'_{n_a}(k_{n_a p_a}) - J'_{n_a}\left(k_{n_a p_a}\frac{R_o}{R_i^B}\right)Y'_{n_a}(k_{n_a p_a})\right] = 0 \tag{9}$$

The mode shapes and the acoustic modal mass for the annular cavity are given by

$$F^B_{m_a n_a p_a} = \Gamma\left(k_{n_a p_a}\frac{r}{R_i^B}\right)\cos(n_a\theta)\cos\left(\frac{m_a\pi}{\ell}z\right) \tag{10}$$

$$M^B_{m_a n_a p_a} = \frac{1}{V^B}\int_0^\ell\int_0^{2\pi}\int_{R_i^B}^{R_o}\left[\Gamma\left(k_{n_a p_a}\frac{r}{R_i^B}\right)\cos(n_a\theta)\cos\left(\frac{m_a\pi}{\ell}z\right)\right]^2 r\,\mathrm{d}r\,\mathrm{d}\theta\,\mathrm{d}z \tag{11}$$

where

$$\Gamma\left(k_{n_a p_a}\frac{r}{R_i^B}\right) \equiv J_{n_a}\left(k_{n_a p_a}\frac{r}{R_i^B}\right) - \frac{J'_{n_a}\left(k_{n_a p_a}\frac{R_o}{R_i^B}\right)}{Y'_{n_a}\left(k_{n_a p_a}\frac{R_o}{R_i^B}\right)}Y_{n_a}\left(k_{n_a p_a}\frac{r}{R_i^B}\right) \tag{12}$$

The integration in Eq. (11) is performed numerically. Equations (7) and (11) help form the acoustic portion of the system mass matrix

whereas Eqs. (6) and (8) are used in the acoustic portion of the system stiffness matrix. Equations (5) and (10) are used in the computation of the coupling coefficients (see Sec. III.C).

B. Structural Model

There exist a variety of analytical models that can be used to describe the vibration of cylindrical shells. Choosing the most appropriate model is often a matter of shell geometry. Leissa [15] provides a detailed survey of the different shell models and their ranges of applicability. Based on the geometry of interest, Flügge's equations are chosen as the structural model (see the Appendix for the complete form of these equations). For a simply supported shell of length ℓ the structural mode shapes can be expressed as follows:

$$\Psi_{m_s n_s} = \left\{ \begin{array}{c} (\partial/\partial z)\cos(n_s\theta) \\ \sin(n_s\theta) \\ \cos(n_s\theta) \end{array} \right\} \sin\left(\frac{m_s \pi}{\ell} z\right) \tag{13}$$

Substituting $\Psi_{m_s n_s} e^{i\Omega t}$ into Flügge's equations leads to the bicubic characteristic equation

$$\bar{\Omega}^6 + d_2\bar{\Omega}^4 + d_1\bar{\Omega}^2 + d_0 = 0 \tag{14}$$

where the coefficients d_0, d_1, and d_2 are lengthy expressions (see the Appendix) which depend on the shell's geometry, Poisson's ratio, and the wave numbers of interest. For a given axial and circumferential wave number, Eq. (14) returns three natural frequencies. The modes corresponding to these frequencies are typically dominated by either axial, circumferential, or radial contributions. The radially dominant natural frequency (generally the lowest of the three) is of interest here because it is the only frequency that is appreciably affected by the presence of the fluid. The formulation of the coupled equations of motion also requires the calculation of the structural modal mass for the cylindrical shell which is given by

$$\begin{aligned} M_{m_s n_s} &= \rho_s h \int_A \left(\Psi^{\text{radial}}_{m_s n_s}\right)^2 \mathrm{d}A \\ &= \rho_s h \int_0^{\ell} \int_0^{2\pi} \left[\cos(n_s\theta)\sin\left(\frac{m_s\pi}{\ell}z\right)\right]^2 a_0 \,\mathrm{d}\theta\,\mathrm{d}z = \frac{1}{\varepsilon_{n_s}}\pi\rho_s h a_0 \ell \end{aligned} \tag{15}$$

To ensure correct implementation of the shell model for this study, outputs were verified using results available in the literature [8,16] and with the finite element software ANSYS.

C. Coupled Equations of Motion

To construct the coupled equations of motion we first expand the radial shell displacement and the velocity potential in terms of their normal modes

$$w = \sum_{m_s=0}^{\infty}\sum_{n_s=0}^{\infty} q_{m_s n_s} \Psi^{\text{radial}}_{m_s n_s} \tag{16}$$

$$\Phi = \sum_{m_a=0}^{\infty}\sum_{n_a=0}^{\infty}\sum_{p_a=1}^{\infty} a_{m_a n_a p_a} F^{A,B}_{m_a n_a p_a} \tag{17}$$

It can now be shown [3,17] that the equations governing the free vibration of the acoustic-structure system of interest are

$$\begin{aligned} &V^A M^A_{m_a n_a p_a}\left[\ddot{a}^A_{m_a n_a p_a} + \left(\varpi^A_{m_a n_a p_a}\right)^2 a^A_{m_a n_a p_a}\right] \\ &\quad = c_0^2 A_F^A \sum_{m_s=1}^{\infty}\sum_{n_s=0}^{\infty} \dot{q}_{m_s n_s} L^A_{m_s n_s m_a n_a p_a} \end{aligned} \tag{18}$$

$$\begin{aligned} &V^B M^B_{m_a n_a p_a}\left[\ddot{a}^B_{m_a n_a p_a} + \left(\varpi^B_{m_a n_a p_a}\right)^2 a^B_{m_a n_a p_a}\right] \\ &\quad = -c_0^2 A_F^B \sum_{m_s=1}^{\infty}\sum_{n_s=0}^{\infty} \dot{q}_{m_s n_s} L^B_{m_s n_s m_a n_a p_a} \end{aligned} \tag{19}$$

$$\begin{aligned} &M_{m_s n_s}[\ddot{q}_{m_s n_s} + (\Omega_{m_s n_s})^2 q_{m_s n_s}] \\ &\quad = \rho_0 \sum_{m_a=0}^{\infty}\sum_{n_a=0}^{\infty}\sum_{p_a=1}^{\infty}\Big(-A_F^A \dot{a}^A_{m_a n_a p_a} L^A_{m_s n_s m_a n_a p_a} \\ &\qquad + A_F^B \dot{a}^B_{m_a n_a p_a} L^B_{m_s n_s m_a n_a p_a}\Big) \end{aligned} \tag{20}$$

where $L^{A,B}_{m_s n_s m_a n_a p_a}$ is the coupling coefficient given by

$$L^{A,B}_{m_s n_s m_a n_a p_a} = \frac{1}{A_F^{A,B}} \int_{A_F^{A,B}} \Psi^{\text{radial}}_{m_s n_s} F^{A,B}_{m_a n_a p_a} \,\mathrm{d}A \tag{21}$$

$L^{A,B}_{m_s n_s m_a n_a p_a}$ can be interpreted as a measure of the spatial similarity between a given acoustic and a structural mode shape. Note the sign difference that exists among the coupling terms in Eqs. (18–20). This difference arises because the normal vector pointing from the shell surface into cavity A points in a direction opposite that of the corresponding vector pointing into cavity B. Substituting the expressions for $\Psi^{\text{radial}}_{m_s n_s}$ and $F^{A,B}_{m_a n_a p_a}$ into Eq. (21) results in two rules (which are applicable to both cavities A and B) regarding the nature of the coupling coefficient. $L^{A,B}_{m_s n_s m_a n_a p_a}$ will be nonzero provided 1) the structural and acoustic circumferential wave numbers are equal (i.e., $n_s = n_a$) and 2) the structural and acoustic axial wave numbers differ by an odd number (i.e., $m_s = m_a \pm 1, m_a \pm 3, m_a \pm 5, \ldots$). In all other cases, the following closed-form expressions are used to calculate the coupling coefficients corresponding to cavities A and B

$$L^A_{m_s n_s m_a n_a p_a} = \frac{J_{n_a}(\alpha'_{n_a p_a}) m_s [(-1)^{m_a+m_s} - 1]}{\varepsilon_{n_s}\pi\left(m_a^2 - m_s^2\right)} \tag{22}$$

$$L^B_{m_s n_s m_a n_a p_a} = \frac{\Gamma(k_{n_a p_a}) m_s [(-1)^{m_a+m_s} - 1]}{\varepsilon_{n_s}\pi\left(m_a^2 - m_s^2\right)} \tag{23}$$

To find the coupled natural frequencies of the system, it is necessary to write Eqs. (18–20) in matrix form and solve the associated eigenvalue problem. Because we wish to consider the $n = 0$ family of modes, it is important to make a small modification to Eqs. (18–20) to prevent computational difficulties. The constant pressure acoustic mode (i.e., $m_a = 0$, $n_a = 0$, $p_a = 1$) in each cavity has a natural frequency of zero. Including these modes as individual elements in the stiffness matrix would cause the matrix to be singular. However, neglecting these modes would ignore the fact that due to the "breathing" nature of the $n = 0$ modes, the presence of the fluid in the cavity effectively stiffens the structure. This is termed the *Helmholtz stiffening effect*. To account for this effect, the method detailed by Bokil and Shirahatti [4] is employed. First, the equation corresponding to the zero frequency mode is eliminated from Eqs. (18) and (19) and then added to Eq. (20). The procedure begins by writing Eqs. (18) and (19) only in terms of the $m_a = 0$, $n_a = 0$, $p_a = 1$ mode. The resulting expression is then integrated with respect to time. It is then noted that near the natural frequency corresponding to the (m_s, n_s) structural mode, the $q_{m_s n_s} L^{A,B}_{m_s n_s 001}$ term will dominate. We can thus closely approximate the summation over m_s and n_s with a single term

$$\dot{a}^A_{001} = \frac{c_0^2 A_F^A}{V^A M^A_{001}} \sum_{m_s=1}^{\infty}\sum_{n_s=0}^{\infty} q_{m_s n_s} L^A_{m_s n_s 001} \approx \frac{c_0^2 A_F^A}{V^A M^A_{001}} q_{m_s n_s} L^A_{m_s n_s 001} \tag{24}$$

$$\dot{a}^B_{001} = -\frac{c_0^2 A_F^B}{V^B M^B_{001}} \sum_{m_s=1}^{\infty} \sum_{n_s=0}^{\infty} q_{m_s 0} L^B_{m_s 0001} \approx -\frac{c_0^2 A_F^B}{V^B M^B_{001}} q_{m_s n_s} L^B_{m_s n_s 001} \tag{25}$$

Multiplying both sides of Eq. (24) by $\rho_0 A_F^A L^A_{m_s n_s 001}$ and both sides of Eq. (25) by $-\rho_0 A_F^B L^B_{m_s n_s 001}$ and then adding the resulting expressions to Eq. (20) gives the following modified equations of motion:

$$V^A M_r^A \left[\ddot{a}_r^A + \left(\varpi_r^A\right)^2 a_r^A\right] = c_0^2 A_F^A \sum_{m_s=1}^{\infty} \sum_{n_s=0}^{\infty} \dot{q}_{m_s n_s} L^A_{m_s n_s r} \quad \text{for } r = 1, 2, 3, \ldots \tag{26}$$

$$V^B M_r^B \left[\ddot{a}_r^B + \left(\varpi_r^B\right)^2 a_r^B\right] = -c_0^2 A_F^B \sum_{m_s=1}^{\infty} \sum_{n_s=0}^{\infty} \dot{q}_{m_s n_s} L^B_{m_s n_s r} \quad \text{for } r = 1, 2, 3, \ldots \tag{27}$$

$$M_{m_s n_s} \ddot{q}_{m_s n_s} + \left(M_{m_s n_s} \Omega^2_{m_s n_s} + \frac{\rho_0 c_0^2 \left(A_F^A\right)^2}{V^A M_0^A} \left(L^A_{m_s n_s 0}\right)^2 + \frac{\rho_0 c_0^2 \left(A_F^B\right)^2}{V^B M_0^B} \left(L^B_{m_s n_s 0}\right)^2\right) q_{m_s n_s} = \rho_0 \sum_{r=1}^{\infty} \left(-A_F^A \dot{a}_r^A L^A_{m_s n_s r} + A_F^B \dot{a}_r^B L^B_{m_s n_s r}\right) \quad \text{for } r = 1, 2, 3, \ldots \tag{28}$$

where the m_a, n_a, p_a indices have been collapsed back into a single index r to illustrate the fact that the $r = 0$ (i.e., $m_a = 0$, $n_a = 0$, $p_a = 1$) mode is not present in Eqs. (26) and (27), nor is it present on the right-hand side of Eq. (28). It is also noted that due to the nature of the coupling coefficients, $L^A_{m_s n_s 0} = L^B_{m_s n_s 0} = 0$ if $n_s \neq 0$. Thus, the modification just made to the equations of motion is only necessary if the analysis is to include the $n = 0$ family of modes. We are now able to express Eqs. (26–28) in a matrix form that is readily solvable

$$[M] \begin{Bmatrix} \ddot{a}_r^A \\ \ddot{a}_r^B \\ \ddot{q}_{m_s n_s} \end{Bmatrix} + [G] \begin{Bmatrix} \dot{a}_r^A \\ \dot{a}_r^B \\ \dot{q}_{m_s n_s} \end{Bmatrix} + [K] \begin{Bmatrix} a_r^A \\ a_r^B \\ q_{m_s n_s} \end{Bmatrix} = \begin{Bmatrix} 0 \\ 0 \\ 0 \end{Bmatrix} \quad \text{for } r = 1, 2, 3, \ldots \tag{29}$$

where

$$[M] = \begin{bmatrix} V^A M_r^A & 0 & 0 \\ 0 & V^B M_r^B & 0 \\ 0 & 0 & M_{m_s n_s} \end{bmatrix} \qquad [G] = \begin{bmatrix} 0 & 0 & -c_0^2 A_F^A \left[L^A_{m_s n_s r}\right] \\ 0 & 0 & c_0^2 A_F^B \left[L^B_{m_s n_s r}\right] \\ \rho_0 A_F^A \left[L^A_{m_s n_s r}\right]^T & -\rho_0 A_F^B \left[L^B_{m_s n_s r}\right]^T & 0 \end{bmatrix}$$
$$[K] = \begin{bmatrix} V^A M_r^A \left(\varpi_r^A\right)^2 & 0 & 0 \\ 0 & V^B M_r^B \left(\varpi_r^B\right)^2 & 0 \\ 0 & 0 & M_{m_s n_s} \Omega^2_{m_s n_s} + \frac{\rho_0 c_0^2 (A_F^A)^2}{V^A M_0^A} (L^A_{m_s n_s 0})^2 + \frac{\rho_0 c_0^2 (A_F^B)^2}{V^B M_0^B} \left(L^B_{m_s n_s 0}\right)^2 \end{bmatrix} \tag{30}$$

Equation (29) represents a linear, homogeneous, conservative, gyroscopic system that can (with some manipulation to render the $[G]$ matrix skew symmetric) be solved using Meirovitch's algorithm [18]. However, we are interested in adding damping and an external forcing to the analysis and therefore must resort to a different solution method which will be discussed in the next section.

IV. Solving the Free and Forced Vibration Problems

In this section we consider a nonconservative Z degree-of-freedom gyroscopic system of the form

$$[M]\ddot{\mathbf{g}}(\mathbf{t}) + [C + G]\dot{\mathbf{g}}(\mathbf{t}) + [K]\mathbf{g}(\mathbf{t}) = \mathbf{Q} \tag{31}$$

where $[M]$, $[G]$, and $[K]$ are the mass, gyroscopic, and stiffness matrices given by Eq. (30), $[C]$ is the damping matrix, $\mathbf{Q}$ is the $Z \times 1$ forcing vector, and $\mathbf{g}$ represents a set of generalized coordinates that may contain both fluid and structural degrees of freedom. Gyroscopic equations of this form are treated in several textbooks on mechanical vibration (see, e.g., Ginsberg [19] or Meirovitch [12]). We seek the response of this system when subject to harmonic forcing. This is accomplished by transforming the system into an uncoupled second-order form.

A. Nonsymmetric Eigenvalue Problem

Here the nonsymmetric eigenvalue problem corresponding to Eq. (31) is presented and solved in a manner similar to Meirovitch [12]. We start by premultiplying Eq. (31) by $[M]^{-1}$ and rewriting the equation in state form

$$\dot{\mathbf{x}}(\mathbf{t}) = [A]\mathbf{x}(\mathbf{t}) + [B]\mathbf{Q} \tag{32}$$

where

$$[A] = \begin{bmatrix} 0 & [I] \\ -[M]^{-1}[K] & -[M]^{-1}[C + G] \end{bmatrix} \qquad [B] = \begin{bmatrix} 0 \\ [M]^{-1} \end{bmatrix} \qquad \mathbf{x}(\mathbf{t}) = \begin{Bmatrix} \mathbf{g}(\mathbf{t}) \\ \dot{\mathbf{g}}(\mathbf{t}) \end{Bmatrix} \tag{33}$$

Assuming solutions of Eq. (32) are of form, $\mathbf{x}(\mathbf{t}) = \mathbf{X}e^{\lambda t}$, the homogeneous part of Eq. (32) can be expressed as a standard algebraic eigenvalue problem,

$$[A]\mathbf{X} = \lambda \mathbf{X} \tag{34}$$

Because A is nonsymmetric, the eigenvectors, $\mathbf{X}_i$, associated with Eq. (34) cannot be orthogonal with respect to A. The $\mathbf{X}_i$ vectors are, however, biorthogonal to the eigenvectors of the adjoint eigenvalue problem which is given by

$$[A]^T \mathbf{Y} = \lambda \mathbf{Y} \tag{35}$$

The two sets of eigenvectors, $\mathbf{X}_i$ and $\mathbf{Y}_j$ (which are sometimes referred to as the right and left eigenvectors, respectively) can be normalized such that they obey the following relations:

$$\begin{aligned} \mathbf{Y}_j^{*T}\mathbf{X}_i &= 2\delta_{ij} \qquad (i,j=1,2,3,\ldots,2Z) \\ \mathbf{Y}_j^{*T}[A]\mathbf{X}_i &= 2\lambda_i\delta_{ij} \qquad (i,j=1,2,3,\ldots,2Z) \end{aligned} \tag{36}$$

The factor of 2 in these relations is used to simplify the transition of the system into a second-order form (see Patil [13]). For systems that contain nonzero damping and gyroscopic terms, solving Eq. (34) results in Z pairs of complex conjugate eigenvalues (i.e., coupled natural frequencies) and eigenvectors

$$\begin{aligned} \lambda_k &= \alpha_k + i\beta_k \qquad \lambda_{Z+k} = \alpha_k - i\beta_k \qquad \mathbf{X}_k = \mathbf{r}_k + i\mathbf{s}_k \\ \mathbf{X}_{Z+k} &= \mathbf{r}_k - i\mathbf{s}_k \qquad \mathbf{Y}_k = \mathbf{u}_k + i\mathbf{v}_k \\ \mathbf{Y}_{Z+k} &= \mathbf{u}_k - i\mathbf{v}_k \qquad (k=1,2,3,\ldots,Z) \end{aligned} \tag{37}$$

B. Determination of Modal Force

Patil [13] developed a procedure for transforming equations in the form of Eq. (31) into a forced uncoupled second-order form. A critical step in this procedure involves calculating a modal force vector that is compatible with the transformed set of equations. To calculate the modal force, consider the original definition of the system eigenvectors found in Eq. (37) and note that multiplying an eigenvector by any complex constant $c_k = c_{k_R} + ic_{k_I}$ will return another system eigenvector. The adjoint eigenvector will then need to be multiplied by the complex conjugate of c_k in order for the two eigenvectors to remain biorthogonal. We also note that the normalization conditions given by Eq. (36) will continue to be true provided $(c_{k_R}^2 + c_{k_I}^2) = 1$. We therefore seek a value of c_k that has a complex modulus equal to unity. It can be shown that the constant must also render a purely imaginary eigenvector when it is multiplied by the original left eigenvector, $\mathbf{Y}_k$. Such a complex constant is given by

$$c_k = \frac{\bar{D}_k^1 - \bar{D}_k^2}{\left[\left(\bar{D}_k^1\right)^2 + \left(\bar{D}_k^2\right)^2\right]^{1/2}} \tag{38}$$

where

$$\bar{D}_k^1 = \{\mathbf{u}_k\}^T[B]\mathbf{Q}, \qquad \bar{D}_k^2 = \{-\mathbf{v}_k\}^T[B]\mathbf{Q} \tag{39}$$

The constant is c_k computed and multiplied by $\mathbf{Y}_k$. Its complex conjugate is then multiplied by $\mathbf{X}_k$. This results in two sets of biorthonormal eigenvectors in the form of those in Eq. (37), but with new values for $\mathbf{r}_k$, $\mathbf{s}_k$, $\mathbf{u}_k$, and $\mathbf{v}_k$. The modal force amplitude vector is then calculated by applying

$$D_k^1 = \{\mathbf{u}_k\}^T[B]\mathbf{Q}, \qquad D_k^2 = \{\alpha_k\mathbf{u}_k - \beta_k\mathbf{v}_k\}^T[B]\mathbf{Q} \tag{40}$$

using the new values of $\mathbf{u}_k$, and $\mathbf{v}_k$. The result is a vector in which $D_k^1 = 0$. This allows for the forced equations of motion to be written in uncoupled, second-order form.

C. Forced Response to Harmonic Excitation

Expressing the response of Eq. (31) in terms of the generalized coordinates $\mathbf{g}$ we have

$$\begin{Bmatrix} \mathbf{g}(\omega) \\ \dot{\mathbf{g}}(\omega) \end{Bmatrix} = \sum_{k=1}^{Z} \frac{D_k^2}{\left(\alpha_k^2 + \beta_k^2\right) - \omega^2 - 2\alpha_k i\omega} \begin{pmatrix} \mathbf{r}_k + \dfrac{i\omega - \alpha_k}{\beta_k}\mathbf{s}_k \end{pmatrix} \tag{41}$$

This expression allows for the direct computation of the amplitude and phase of the response at any forcing frequency, ω. At this point it is important to recall that the generalized structural coordinates $q_{m_s n_s}$ (which comprise a portion of the $\mathbf{g}$ vector) are related to the shell's radial displacement, w, by the modal expansion

$$w(\theta,z,\omega) = \sum_{m_s=1}^{M_s}\sum_{n_s=0}^{N_s} q_{m_s n_s}(\omega)\Psi_{m_s n_s}^{\text{radial}}(\theta,z) \tag{42}$$

After Eq. (41) is applied to determine the amplitude of the response associated with each generalized coordinate, it is necessary to compute the shell deflection at a given point using Eq. (42).

V. Results and Discussion

In this section the foregoing theoretical model is used to calculate the system frequencies and forced response of cylindrical shells loaded with LH_2 and LOX.

A. Coupled System Frequencies

The natural frequencies of the fluid-structure system are found for four different configurations. In Fig. 2, the shell is coupled to LH_2 ($c_0 = 1040$ m/s and $\rho_0 = 70$ kg/m^3) enclosed in a simple cylindrical duct (cavity A). No exterior fluid is assumed in this case. The converse is true in Fig. 3 where LH_2 resides in the annular cavity (cavity B) only. In Fig. 4, the shell is coupled to LH_2 in both cavities A and B. Figure 5 considers both cavities A and B to be filled with LOX ($c_0 = 1008$ m/s and $\rho_0 = 1140$ kg/m^3). In all cases, the shell has geometry and material properties consistent with that of the

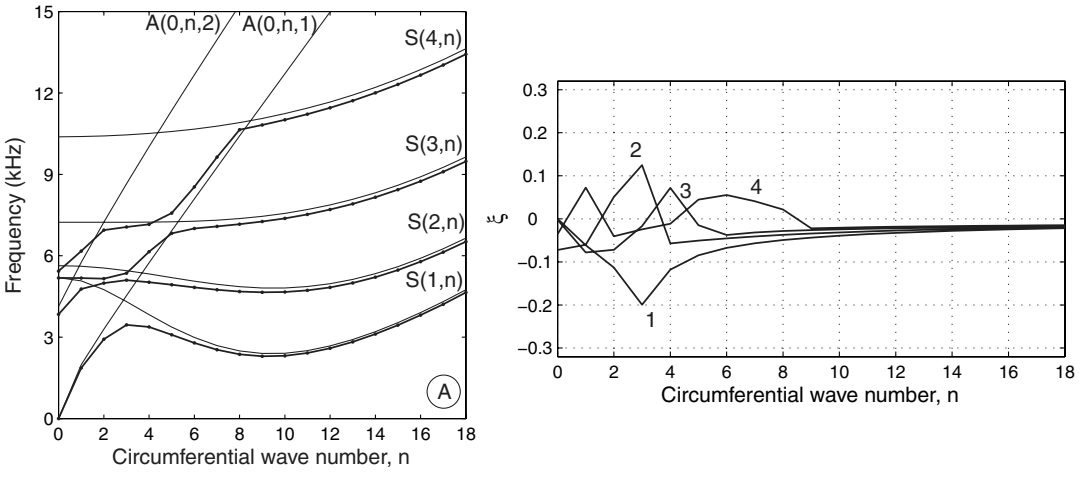

a) b)

Fig. 2 System frequency behavior for cylindrical shell with interior fluid only. a) Four lowest system frequencies (solid lines with data markers) plotted with rigid wall acoustic cavity frequencies and in vacuo structural frequencies (solid lines without data markers). Indices are denoted in the following order: axial, circumferential, radial. b) Veering diagram for four lowest system frequencies (numbered in ascending order).

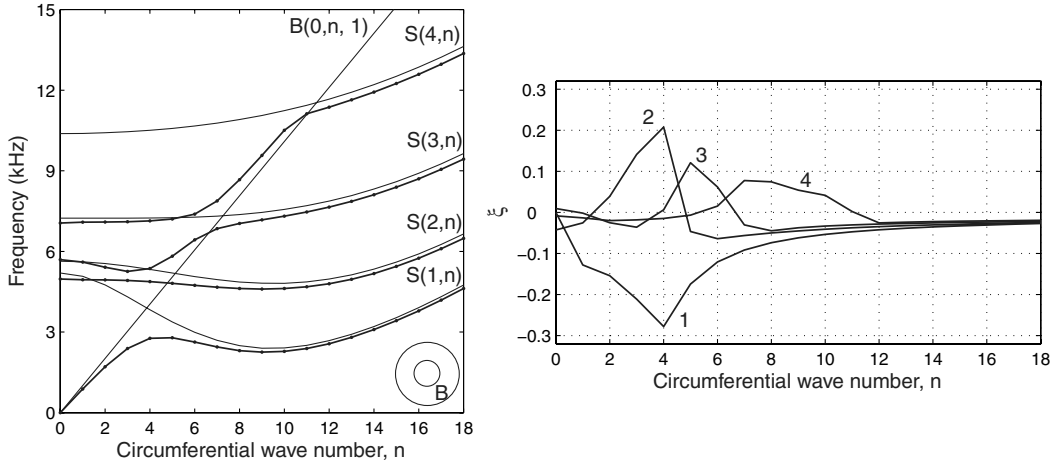

a) b)

Fig. 3 System frequency behavior for cylindrical shell with bounded exterior fluid only. a) Four lowest system frequencies b) veering diagram.

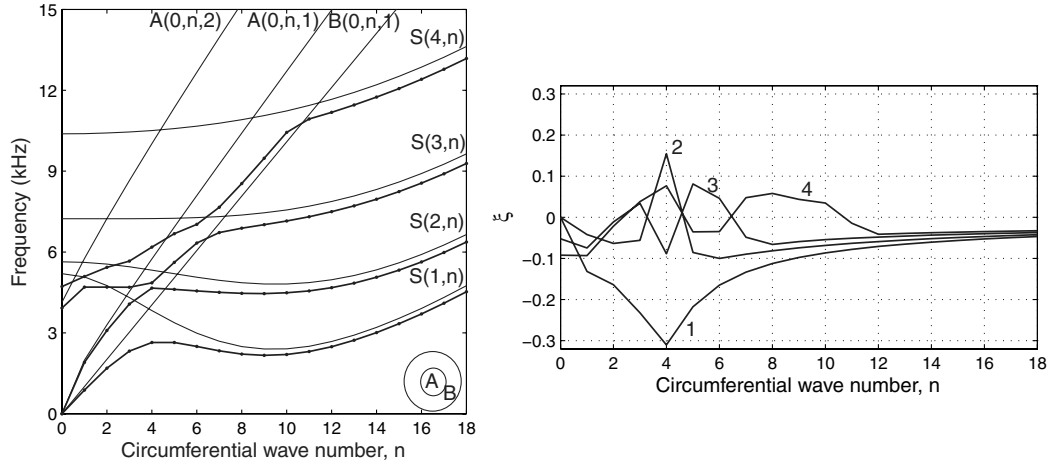

a) b)

Fig. 4 System frequency behavior for cylindrical shell with both interior and bounded exterior fluids. a) Four lowest system frequencies b) veering diagram.

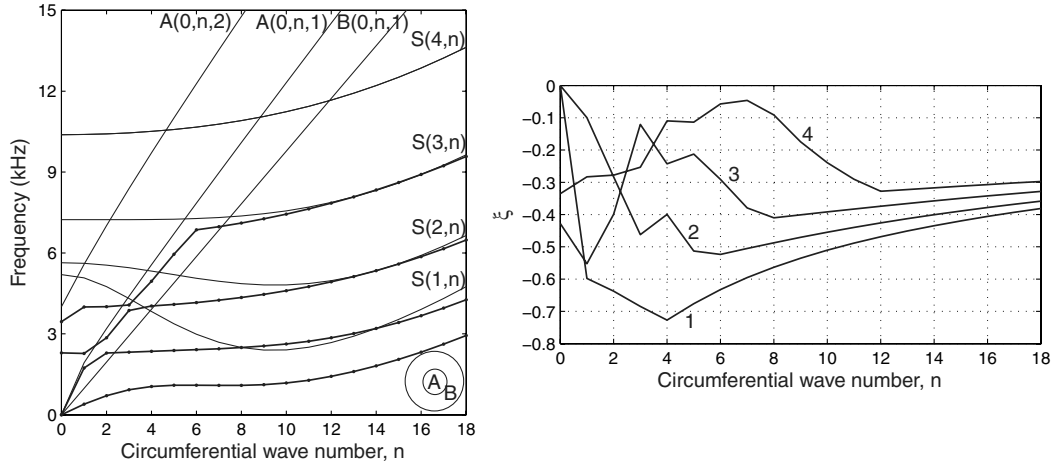

a) b)

Fig. 5 System frequency behavior for cylindrical shell with LOX on the interior and bounded exterior. a) Four lowest system frequencies b) veering diagram.

Orbiter downstream gimbal joint flowliner. The inner and outer cavity radii, R_i and R_o, are 15.33 and 17.36 cm, respectively. The shell length is 7.31 cm and its thickness is 1.27 mm. The shell material is Inconel 718 ($E = 204.9$ GPa, $\nu = 0.29$, $\rho_s = 8190$ kg/m^3). Because only equivalent circumferential wave numbers couple, the equations of motion in each case are constructed for one value of n at a time.

Parts A of Figs. 2–5 display the four lowest system frequency branches as well as the four lowest in vacuo structural frequency branches. Also included are any rigid wall acoustic frequency curves

that may exist within the frequency range of interest. The frequency curves corresponding to cavities A and B are denoted with the appropriate letter. The in vacuo structural frequency branches are denoted with the letter S. All system and in vacuo structural frequencies displayed are radial in nature. Any predominately circumferential and/or axial frequencies that may exist within the displayed frequency range are not of interest here because they do not couple appreciably to the fluid. All displayed frequencies are undamped.

Eigenvalue veering can be observed near certain intersections of rigid wall acoustic and in vacuo structural frequencies. Near these intersections, the system natural modes are well coupled and receive significant contribution in terms of energy from both the acoustic cavity and the structure. Away from the intersections, the system is only lightly coupled and exhibits modes that are dominated by a contribution from either a rigid wall acoustic mode or an in vacuo structural mode. In this system, eigenvalue veering occurs only when intersecting frequencies have a nonzero coupling coefficient (i.e., the axial wave numbers associated with the two intersecting frequencies differ by an odd number). For example, observe the apparent lack of curve veering demonstrated by the second branch of system frequencies in Fig. 3 near the intersection of the $S(2, n)$ and the $B(0, n, 1)$. It is evident from Fig. 4 that the effect of the annular backing cavity is manifested by the presence of additional acoustic modes with which the structural modes may couple.

Parts B of Figs. 2–5 quantify the amount of eigenvalue veering undergone by each of the four branches of system frequencies. These plots depict the frequency shift parameter, ξ, for the four lowest branches of system frequencies. ξ quantifies the percentage difference between a coupled system frequency and its nearest uncoupled acoustic or structural frequency. Because they combine to produce the overall system behavior, these uncoupled frequencies are termed *component frequencies*. For a given circumferential wave number, ξ is calculated by taking the difference between a coupled frequency and its nearest acoustic or structural component frequency and then dividing the difference by said component frequency. Figure 4b illustrates that introducing the shell of interest into an environment of LH_2 can result in system frequencies that are as much as 30% lower than the nearest component frequency. Although the largest frequency shifts occur near certain intersections of two component frequencies, it is important to note that ξ incorporates both the effects of acoustic-structure coupling as well as any hydrodynamic mass effects. It is these hydrodynamic mass effects that are responsible for ξ approaching a value less than zero for high values of n. In other words, for system natural frequencies that are not near an intersection of two component frequencies, the added mass due to the fluid is the primary cause of any frequency shift. In the case of LH_2, hydrodynamic mass effects alone cause system frequencies to be approximately 5% lower than the corresponding in vacuo structural frequency. With a density about 16 times that of LH_2, the hydrodynamic mass effects associated with LOX are much more pronounced. Figure 5 demonstrates that for high values of n, the hydrodynamic mass effects are responsible for a 30–40% frequency reduction. Near the intersection of the $S(1, n)$ and the $B(0, n, 1)$ modes, the natural frequency of the shell-LOX system is over 70% lower than the closest component frequency. The fact that the third and fourth system frequency branches in Fig. 5 appear to closely follow the second and third branches of in vacuo structural frequencies is thought to be a coincidence due to the geometry and physical properties of the system being considered.

B. Convergence of System Frequencies

It is not immediately evident how many acoustic modes need to be retained to ensure adequate convergence of a given branch of system frequencies, nor is it obvious the extent to which fluid properties affect convergence rates. Figures 6a and 6b show the convergence results for the first four branches of system frequencies displayed in Figs. 4 and 5, respectively. Convergence is plotted with respect to K, a parameter which represents the index number of the highest-order axial or radial acoustic mode retained (i.e., $K = M_a = P_a$). Convergence at a given value of K is defined as the percent difference between the frequencies computed at K and $K + 1$. Convergence for each branch of frequencies is computed for circumferential wave numbers ranging from zero to 18. The mean of these 19 convergence values is computed and plotted in Fig. 6. Recalling that there are two acoustic cavities of interest and noting that the axial acoustic mode indices begin with zero whereas the radial acoustic mode indices begin with 1, the total number of acoustic modes retained for any given circumferential wave number is $2K(K + 1)$. It is clear that for a given value of K, the frequency convergence percentages are at least 5 times higher for LOX filled cavities than they are for cavities filled with LH_2. In the case of LOX, the modal masses of the higher-order acoustic modes are relatively large due to the fluid's high density. Thus, more of these modes need to be retained to obtain a desired level of convergence. For both LH_2 and LOX, however, when $K > 5$ the utility of retaining additional acoustic basis functions is significantly diminished. All system frequency and forced response curves presented here are generated using a K value of at least 5.

C. Structural Forced Response

Before turning attention to the forced response of the submerged structure, it is instructive to consider the nature of the coupled system modes and how they differ from the corresponding uncoupled component modes. Figure 7 compares coupled and uncoupled modes for three representative cases. Figure 7a depicts a system mode dominated by contributions from the $m_a = 0$, $n_a = 1$, $p_a = 1$ acoustic cavity mode while Fig. 7b shows a system mode receiving

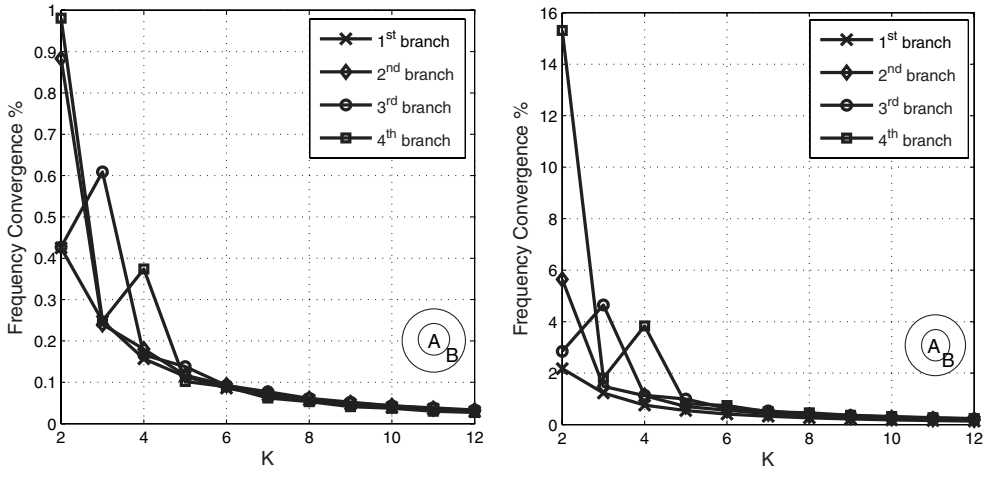

Fig. 6 Average percentage frequency convergence ratios for cases where cavities A and B are filled with a) LH_2 and b) LOX.

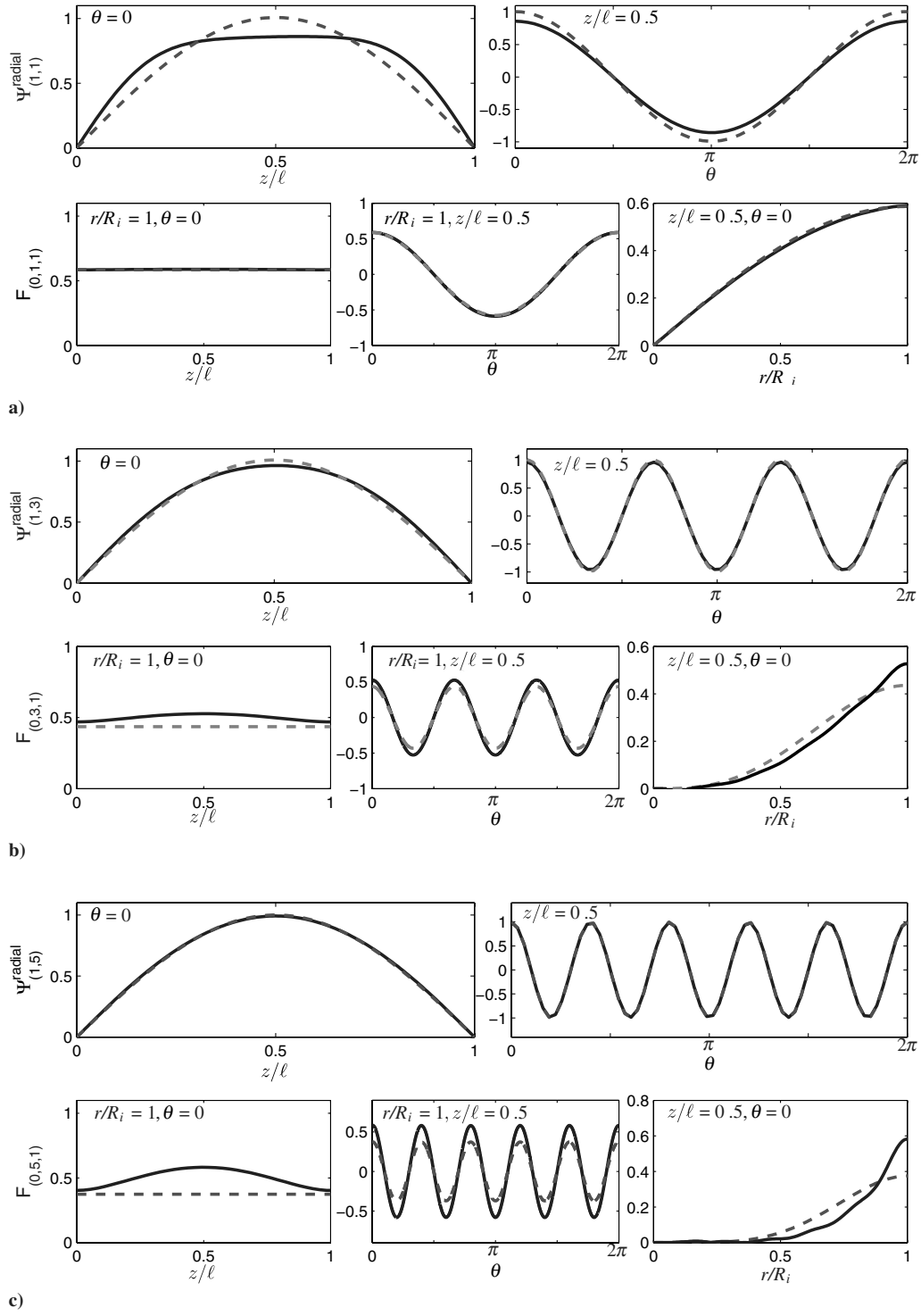

Fig. 7 Comparison of coupled (solid lines) and uncoupled (dashed lines) mode shapes for a cylindrical with LH_2 residing in cavity A only. a) A system mode dominated by contributions from the $m_a = 0$, $n_a = 1$, $p_a = 1$ cavity mode. b) A system mode receiving significant contributions from the $m_a = 0$, $n_a = 3$, $p_a = 1$ cavity mode and the $m_s = 1$, $n_s = 3$ structural mode. c) A system mode dominated by contributions from the $m_s = 1$, $n_s = 5$ structural mode.

significant contributions from both the $m_a = 0$, $n_a = 3$, $p_a = 1$ cavity mode and the $m_s = 1$, $n_s = 3$ structural mode. In Fig. 7c, the system mode is dominated by contributions from the $m_s = 1$, $n_s = 5$ uncoupled structural mode. In each of these cases, the cylinder contains LH_2 in cavity A. The coupled frequencies corresponding to these three cases can be found on the lowest branch of system frequencies shown in Fig. 2a. The coupled and uncoupled structural mode shapes are shown in the upper two plots in Figs. 7a–7c and are both normalized according to Eq. (15). The bottom three plots in each part depict the coupled and uncoupled acoustic mode shapes and are normalized according to Eq. (7).

By inspection of the analytical expressions for the uncoupled acoustic and structural mode shapes [Eqs. (5) and (13), respectively], it is evident that at the fluid-structure interface, the two expressions differ in terms of their axial dependence. The structure exhibits an axial dependence of $\sin[(m_s\pi/\ell)z]$ while the acoustic cavity has an axial dependence of $\cos[(m_a\pi/\ell)z]$. Thus for the cases shown in Fig. 7 where a $m_a = 0$ branch of uncoupled acoustic modes intersects with a $m_s = 1$ branch of structural modes, the axial dependence of the uncoupled acoustic modes will be a uniform constant while that of the uncoupled structural modes will be a half sine wave. In the coupled case, the system modes exhibit axial dependencies that are

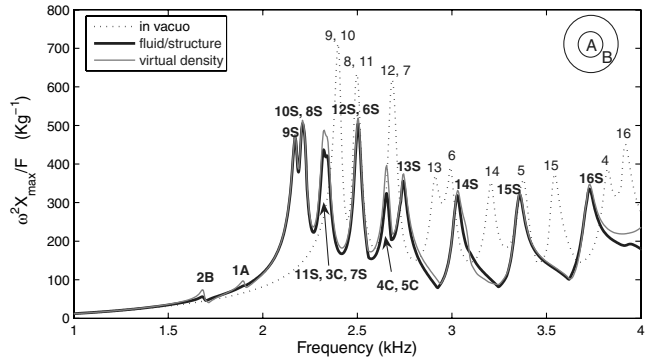

Fig. 8 Forced response of cylindrical shell with LH_2 in both cavities *A* and *B*. Peaks are indicated with their corresponding circumferential wave number followed by an "A," "B," "S," or "C." A and B indicate that the corresponding mode is a primarily acoustic mode associated with either cavity *A* or *B*. S indicates a primarily structural mode and C denotes modes where strong acoustic-structural coupling exists.

some combination of these two uncoupled shapes. How the uncoupled shapes ultimately combine depends upon whether the system mode is dominated by the cavity or the structure. For instance, if a given system mode is cavity dominated, the acoustic portion of the system mode is virtually identical to its uncoupled counterpart. However, the axial dependence of the structural coupled mode shape differs significantly from the uncoupled half sine wave shape due to the significant contribution from the uncoupled acoustic mode. This is evidenced by the top left plot of Fig. 7a. The converse of this situation is clear in Fig. 7c. Figure 7b illustrates a case where the coupled mode shapes receive noticeable contributions from both the acoustic and structural uncoupled mode shapes.

Figures 8 and 9 show the response of the shell subject to a harmonic point excitation at an axial position located approximately one-third down the length of the shell ($z \approx L/3$) and at a circumferential location given by $\theta = 0$. Note that this axial position is near a node for the third branch ($m_s = 3$) of structural modes; thus these modes are not appreciably excited by the point source. However, the natural frequencies associated with these $m_s = 3$ modes are well above the frequency range of interest for this example. To better illustrate the relative magnitudes of the resonant peaks, a constant damping ratio of 0.7% is applied across all system modes. This low value of damping is consistent with tests performed on the Space Shuttle Orbiter gimbal joint flowliners. This constant damping ratio was applied by first solving the undamped eigenvalue problem [i.e., $[C] = 0$ in Eq. (31)]. Next, the real part of the eigenvalues are approximated as the product of the damping ratio and the imaginary part of the eigenvalues (i.e., $\alpha_k \approx \zeta\beta_k$). This approximation neglects any reduction in natural frequency due to damping, but given the very low damping ratio considered here, this reduction is trivially small. The computed values for α_k are then used in Eq. (41) to calculate the overall system response.

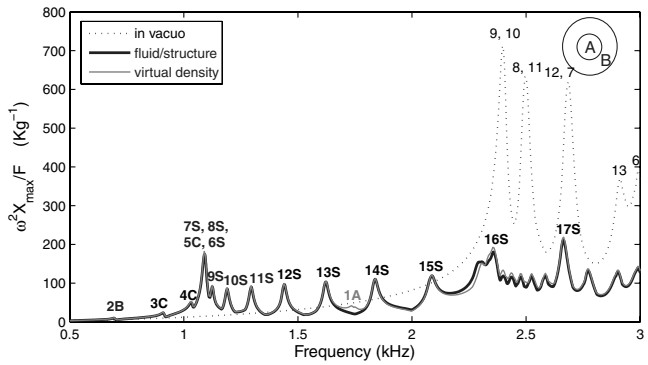

Fig. 9 Forced response of cylindrical shell with LOX in both cavities *A* and *B*.

To properly assess the relative amplitude of the resonant peaks it is necessary to calculate the system response at and in the vicinity of each resonant frequency. This is accomplished by building a vector of forcing frequencies at which the response is to be evaluated. This vector contains every frequency (within a predefined range) at which the response is thought to be a local maximum. In the case of a forced single degree-of-freedom (SDOF) oscillator, the maximum response will occur at frequency equal to $\omega_{\text{nat}}\sqrt{1-2\zeta^2}$. Thus, the forcing vector contains evaluation points at and around values consistent with this expression. The vector also contains many intermediate frequencies spaced at intervals no greater than 5 Hz.

In both Figs. 8 and 9, the response is evaluated at a range of points across the entire surface of the shell. The maximum amplitude of radial displacement at a given forcing frequency is then retained and denoted $X_{\max}$. Tracking the maximum displacements in this manner is considered preferable to calculating the displacements at a single prescribed location because in the latter case, the relative amplitude of the resonant peaks will be dependent upon the chosen location. The forced response is plotted in terms of $\omega^2 X_{\max}/F$. This parameter is chosen because it elucidates the added mass effects associated with the fluid. This fact can be observed by considering the response of a SDOF oscillator. In a SDOF system, the $\omega^2 X_{\max}/F$ parameter will attain a maximum value of approximately $1/(2\zeta m)$ where m is the mass of the oscillator.

Figures 8 and 9 each show three response curves. The dotted curves correspond to the response of the structure in vacuo. These curves are generated using conventional modal analysis techniques for self-adjoint systems. The dark solid curves represent the response of the fluid-structure system and are calculated using the approach described in Sec. IV. The solid gray curves help reveal the effects associated with the fact that the natural modes in the fluid-structure system possess contributions from both the fluid and the structure. These so-called "virtual density" curves are produced by first calculating the fluid-structure system frequencies that are shown in Figs. 4 and 5. Next, it is assumed that the fluid contributes only additional mass to the system and not any additional stiffness. With this assumption it is possible to calculate virtual density factors for each system mode. These factors are given by $(\Omega_{m_s n_s}/\omega_{m_s n_s})^2$, where $\omega_{m_s n_s}$ are the natural frequencies of the coupled fluid-structure system. For each mode, the corresponding virtual density factor is multiplied by the actual physical density of the structure. The result is a pseudostructure that possesses natural frequencies that are equivalent to the fluid-structure frequencies. The forced response of the pseudostructure is then evaluated using conventional modal analysis techniques for self-adjoint systems. The results indicate that the virtual density curves closely follow the fluid-structure curves in most cases. However, it is clear from Fig. 8 that the virtual density curve overestimates the response in cases where the system is being forced near frequencies corresponding to either acoustically dominated or strongly coupled modes. Because the virtual density curves only contain structural modal content, the difference between the virtual density and the fluid-structure curves isolates the effect that the coupled natural modes of the fluid-structure system have on the structural response. The correspondence between the virtual density curve and the fluid-structure curve in Fig. 9 is even stronger. This confirms the notion that in the case of the structural forced response, the hydrodynamic mass effects of the LOX dominate any effects that may be due to acoustic-structure coupling.

Figures 8 and 9 also demonstrate how the order of the modes changes significantly in the presence of fluid. It is clearly possible for two modes that are well separated in the in vacuo case to become quite near each other in the fluid case and vice versa. In fact, it would be difficult to infer any useful information about the forced response of a structure submerged in LH_2 or LOX by only considering the response of the structure in vacuo.

VI. Conclusions

The results of this study demonstrate that submerging a typical engineering structure in LH_2 or LOX can dramatically alter the structure's free and forced response. Accurately predicting these

fluid effects has long been a challenge to engineers at NASA and the broader community. Historically, analysts have used empirically derived "knockdown factors" to estimate natural frequencies of a fluid-structure system. Although the use of such factors may be justified in some cases, they are likely to be highly dependant upon system geometry and are thus not suitable for general application. The use of knockdown factors also belies the inherent complexity of fluid-structure systems by obscuring the contribution of individual acoustic and structural modes. The frequency plots and veering diagrams in this study prove that if the rigid wall acoustic frequencies are comparable to the in vacuo structural frequencies, the resulting system frequency behavior can be complicated and difficult to generalize. In situations where the dynamics of structures connected to cavities containing LH_2 or LOX are of interest, it seems imperative that the analyst at least perform calculations to determine whether or not the acoustic natural frequencies of the cavity are comparable to the corresponding structural natural frequencies. If the physical configuration is such that the acoustic and structural frequencies do not coincide near the forcing frequencies of interest, simpler theoretical models that account for the mass loading due to the fluid can be applied. If the acoustic and structural frequencies are comparable, however, studies using approaches similar to the one presented here may be necessary.

Appendix: Shell Equations of Motion

The Flügge equations of motion for the middle surface of a cylindrical shell in vacuo are given by

$$u'' + \frac{1-\nu}{2}u^{\cdot\cdot} + \frac{1+\nu}{2}v^{\prime\cdot} + \nu w' + \sigma\left(\frac{1-\nu}{2}u^{\cdot\cdot} - w''' + \frac{1-\nu}{2}w^{\prime\cdot\cdot}\right) = \gamma\frac{\partial^2 u}{\partial t^2} \tag{A.1}$$

$$\frac{1+\nu}{2}u^{\prime\cdot} + v^{\cdot\cdot} + \frac{1-\nu}{2}v'' + w^{\cdot} + \sigma\left(\frac{3}{2}(1-\nu)v'' - \frac{3-\nu}{2}w^{\prime\prime\cdot}\right) = \gamma\frac{\partial^2 v}{\partial t^2} \tag{A.2}$$

$$\nu u' + v^{\cdot} + w + \sigma\left(\frac{1-\nu}{2}u^{\prime\cdot\cdot} - u''' - \frac{3-\nu}{2}v^{\prime\prime\cdot} + \nabla^4 w + 2w^{\cdot\cdot} + w\right) = -\gamma\frac{\partial^2 w}{\partial t^2} \tag{A.3}$$

where

$$\sigma = \frac{1}{12}\left(\frac{h}{a_0}\right)^2 \tag{A.4}$$

$$\gamma = \rho_s a_0^2\frac{(1-\nu^2)}{E} \tag{A.5}$$

and where

$$\nabla^2 = a_0^2\frac{\partial^2(\,)}{\partial z^2} + \frac{\partial^2(\,)}{\partial\theta^2}$$

is the dimensionless form of the standard Laplacian with

$$\frac{\partial(\,)}{\partial r} = 0$$

Substituting the mode shapes given by Eqs. (13) into Eqs. (A.1), (A.2), and (A.3) yields a characteristic equation [Eq. (14)] with the following coefficients:

$$d_2 = \tfrac{1}{2}\Big[n_s^2(\nu-3) + \mu^2(\nu-3) - 2 + \sigma\Big(-2n_s^4 - 2\mu^4 + 3\mu^2(\nu-1) + n_s^2(3-4\mu^2+\nu) - 2\Big)\Big] \tag{A.6}$$

$$d_1 = \tfrac{1}{4}\Big[2\sigma n_s^6(\sigma-(1+\sigma)\nu+3) + 2\mu^2\Big(3\sigma(\mu^4+\mu^2+2) - \sigma\nu(\mu^4+7\mu^2+4) + (1-\nu)(\mu^2+2\nu+3) + \sigma^2(\mu^4-3(1+\mu^4)\nu+3)\Big) - n_s^4\Big(2\sigma(5+3\mu^2(\nu-3)-\nu) + 2(\nu-1) + \sigma^2(\nu-1)(\mu^2(\nu+9)-4)\Big) + n_s^2(\sigma(4\mu^2(\nu-5) - 6\mu^4(\nu-3) - 4\nu + 8) - 2(2\mu^2+1)(\nu-1) + \sigma^2(2-2\nu+3\mu^2(\nu-1)(3+\nu) - \mu^4(\nu^2+12\nu-9)))\Big] \tag{A.7}$$

$$d_0 = \frac{(1-\nu)}{4}\Big[2\mu^4(\nu^2-1) - 2\sigma\Big(n_s^8 + n_s^6(4\mu^2-2) + n_s^4(6\mu^4+2\mu^2(\nu-4)+1) + 2n_s^2\mu^2(2\mu^4-3\mu^2-\nu+2) + \mu^4((\mu^2-3\nu)(\mu^2+\nu)+4)\Big) + \sigma^3\mu^2\Big(6\mu^6 + 3n_s^6(\nu-1) + 3n_s^2(1+3\mu^4)(\nu-1) + 2n_s^4(\nu(\mu^2\nu-3)+3)\Big) + \sigma^2\Big(-2n_s^8 + 2n_s^4(3\mu^4(\nu-2) + \mu^2(7-5\nu) - 1) - 2\mu^4(2\mu^4 - 6\mu^2\nu + 3) + n_s^6(\mu^2(3\nu-7)+4) + n_s^2\mu^2(-7+7\nu+\mu^4(3\nu-11) + 6\mu^2(\nu^2-\nu+2))\Big)\Big] \tag{A.8}$$

where

$$\mu = \frac{m_s\pi a_0}{\ell} \tag{A.9}$$

Acknowledgment

The support of the NASA Graduate Student Researcher Program (GSRP) contract no. NNM05ZA07H is gratefully acknowledged.

References

[1] Frady, G. P., "The Role of Structural Dynamics and Testing in the Shuttle Flowliner Crack Investigation," AIAA Paper 2005-1862, 2005.

[2] Warburton, G. B., "Vibration of a Cylindrical Shell in an Acoustic Medium," *Journal of Mechanical Engineering Science*, Vol. 3, No. 1, 1961, pp. 69–79. doi:10.1243/JMES_JOUR_1961_003_011_02

[3] Dowell, E. H., Gorman, G. F., and Smith, D. A., "Acoustoelasticity: General Theory, Acoustic Natural Modes and Forced Response to Sinusoidal Excitation Including Comparisons with Experiment," *Journal of Sound and Vibration*, Vol. 52, No. 4, 1977, pp. 519–542. doi:10.1016/0022-460X(77)90368-6

[4] Bokil, V. B., and Shirahatti, U. S., "A Technique for the Modal Analysis of Sound-Structure Interaction Problems," *Journal of Sound and Vibration*, Vol. 173, No. 1, 1994, pp. 23–41. doi:10.1006/jsvi.1994.1215

[5] Dowell, E. H., "Interior Noise Studies for Single-And Double-Walled Cylindrical Shells," *Journal of Aircraft*, Vol. 17, No. 9, 1980, pp. 690–699.

[6] Kang, N., and Raman, A., "Aeroelastic Flutter Mechanisms of a Flexible Disk Rotating in an Enclosed Compressible Fluid," *Journal of Applied Mechanics*, Vol. 71, No. 1, 2004, pp. 120–130. doi:10.1115/1.1631034

[7] Junger, M. C., and Feit, D., *Sound, Structures, and Their Interaction*, Acoustical Society of America, Melville, NY, 1993.

[8] Au-Yang, M. K., "Free Vibration of Fluid-Coupled Coaxial Cylindrical Shells of Different Lengths," *Journal of Applied Mechanics*, Vol. 43, Sept. 1976, pp. 480–484.

[9] Gardonio, P., Ferguson, N. S., and Fahy, F. J., "A Modal Expansion Analysis of Noise Transmission Through Circular Cylindrical Shell Structures with Blocking Masses," *Journal of Sound and Vibration*,

Vol. 244, No. 2, 2001, pp. 259–297.
doi:10.1006/jsvi.2000.3456
[10] Kruntcheva, M. R., "Acoustic-Structural Responances of Thin-Walled Structure-Gas Systems," *Journal of Vibration and Acoustics*, Vol. 128, No. 6, 2006, pp. 722–731.
doi:10.1115/1.2345679
[11] Molisani, L., "A Coupled Tire Structure-Acoustic Cavity Model," Ph.D. Thesis, Virginia Polytechnic Institute and State University, Blacksburg, VA, 2004.
[12] Meirovitch, L., *Principles and Techniques of Vibrations*, Prentice–Hall, Upper Saddle River, NJ, 1997.
[13] Patil, M. J., "Decoupled Second-Order Equations and Modal Analysis of a General Non-Conservative System," AIAA Paper 2000-1654, 2000.
[14] Blackstock, D. T., *Fundamentals of Physical Acoustics*, Wiley, New York, 2000.
[15] Leissa, A. W., *Vibration of Shells*, SP-288, NASA, U.S. Government Printing Office, Washington, D.C., 1973.
[16] Amabili, M., and Dalpiaz, G., "Breathing Vibrations of a Horizonatal Circular Cylindrical Tank Shell Partially Filled with Liquid," *Journal of Vibration and Acoustics*, Vol. 117, No. 2, 1995, pp. 187–191.
[17] Dowell, E. H., and Tang, D., *Dynamics of Very High Dimensional Systems*, World Scientific, River Edge, NJ, 2003.
[18] Meirovitch, L., "A New Method of Solution of the Eigenvalue Problem for Gyroscopic Systems," *AIAA Journal*, Vol. 12, No. 10, 1974, pp. 1337–1342.
[19] Ginsberg, J. H., *Mechanical and Structural Vibrations Theory and Applications*, Wiley, New York, 2001.

M. Ahmadian
Associate Editor